NIH Public Access
Author Manuscript
Ann Biomed Eng. Author manuscript; available in PMC 2014 November 01.

Published in final edited form as:
Ann Biomed Eng. 2013 November ; 41(11): . doi:10.1007/s10439-013-0901-8.

Can molecular imaging enable personalized diagnostics? An example using magnetomotive photoacoustic imaging

Matthew O'Donnell[1], **Chen-wei Wei**[1], **Jinjun Xia**[1], **Ivan Pelivanov**[1,2], **Congxian Jia**[1], **Sheng-Wen Huang**[1], **Xiaoge Hu**[1], and **Xiaohu Gao**[1]

[1] Department of Bioengineering, University of Washington 3720, 15th AVE NE, Seattle, WA 98195, USA

[2] Physics Faculty of M.V. Lomonosov Moscow State University Leninskie Gory, 1, bld.2, 119991, Moscow, Russia

Abstract

The advantages of photoacoustic imaging, including low cost, non-ionizing operation, and sub-mm spatial resolution at centimeters depth, make it a promising modality to probe nanoparticle-targeted abnormalities in real time at cellular and molecular levels. However, detecting rare cell types in a heterogeneous background with strong optical scattering and absorption remains a big challenge. For example, differentiating circulating tumor cells *in vivo* (typically fewer than 10 cells/ml for an active tumor) among billions of erythrocytes in the blood is nearly impossible. In this paper, a newly developed technique, magnetomotive photoacoustic (mmPA) imaging, which can greatly increase the sensitivity and specificity of sensing targeted cells or molecular interactions, is reviewed. Its primary advantage is suppression of background signals through magnetic enrichment/manipulation with simultaneous photoacoustic detection of magnetic contrast agent targeted objects. Results from phantom and *in vitro* studies demonstrate the capability of mmPA imaging to differentiate regions targeted with magnetic nanoparticles from the background, and to trap and sensitively detect targeted cells at a concentration of a single cell per milliliter in a flow system mimicking a human peripheral artery. This technique provides an example of the ways in which molecular imaging can potentially enable robust molecular diagnosis and treatment, and accelerate the translation of molecular medicine into the clinic.

Keywords

Personalized healthcare; targeted molecular diagnosis and therapy; composite contrast agent; multifunctional nanoparticle; background suppression; circulating tumor cells

Introduction

Currently, healthcare spending represents almost 18% of the United States Gross Domestic Product (GDP) and is growing rapidly[2], with projections by the CMS that it will reach 20% of GDP by 2021 if allowed to grow at the current rate. The vast majority of current healthcare dollars goes to treatment, with only a small fraction of total expenditures devoted to prediction, diagnosis, and treatment monitoring. Traditional methods of disease management are reactive - we wait until someone is sick before treating the disease with

odonnel@uw.edu Phone: 206-685-2000, Fax: 206-685-3300, cwwei28@uw.edu, xiajj@u.washington.edu, ivanp3@u.washington.edu Tel.: 939-53-09, Fax: 939-31-13, congxianjia@yahoo.com, shengwen.huang71@gmail.com, xiaogehu@u.washington.edu, xgao@u.washington.edu

NIH-PA Author Manuscript
NIH-PA Author Manuscript
NIH-PA Author Manuscript

NIH-PA Author Manuscript

NIH-PA Author Manuscript

NIH-PA Author Manuscript

expensive procedures. A radical departure from this approach is required to reduce overall costs.

One of the keys to cost containment is to shift from diagnosing symptomatic patients to detecting disease in a presymptomatic population, i.e. to shift to personalized healthcare delivery. As shown in Figure 1, personalized healthcare enabled by molecular medicine will be predictive and preventative, probing an individual's unique biology (block 1) to assess the probability of developing various diseases and then designing appropriate treatments, even before the onset of symptoms[8, 32]. This potential transformation of healthcare delivery can radically shift how the nation's healthcare dollar will be used, reducing the percentage spent on treatment and substantially increasing the percentage spent on prediction and diagnosis with the possibility that the overall costs of healthcare delivery can be significantly reduced. The fundamental hypotheses driving the molecular imaging studies detailed in the rest of this article are: (1) personalized medicine will significantly improve healthcare delivery with the potential to simultaneously reduce costs; (2) molecular imaging and therapy are critical to this paradigm; and (3) ultrasound will be one of the major enablers of molecular imaging and therapy.

Most work to date in molecular diagnostics for disease detection has focused on identifying disease biomarkers present in the blood or other easily obtainable bodily fluids[8]. Developing comprehensive, yet personalized assays for diverse populations, however, is highly complex and expensive. An alternate approach is to instead focus on molecular screening, in which molecular tests based on blood-borne biomarkers are tuned for high sensitivity but relatively low specificity. Under this model, depicted in Figure 1, molecular screening (block 3) first identifies a high risk individual. Screening results are augmented by highly specific molecular imaging tests to confirm disease onset, characterize the disease, and/or determine its location (block 4). Finally, molecular therapies can be delivered noninvasively, or with minimal invasion, and molecular imaging can be used to both guide procedures and assess treatment efficacy (block 5). This integrated approach, including several feedback loops specific to the patient, will be more efficient and reliable as highly specific imaging can greatly reduce false positives. Overall, it will help translate molecular diagnostics into a robust personalized tool.

Molecular Imaging

In the past 30 years, medical imaging has dramatically altered medical practice and outcomes. Molecular imaging has the potential to shape the emerging field of personalized medicine with the same dramatic impact. Molecular imaging probes molecular abnormalities driving disease processes rather than the consequences of these molecular alterations. It can be broadly defined as localized *in vivo* characterization and measurement of biologic processes at the cellular and molecular level. Localization will be very important in both diagnostic molecular imaging and image-guided molecular therapies.

Because molecules themselves are generally too small to be imaged directly with noninvasive techniques, specific and sensitive site-targeted probes (or contrast agents) are typically employed as beacons to depict epitopes of interest. And, unlike traditional blood pool contrast agents, a site-targeted agent is intended to enhance a selected biomarker that otherwise might be impossible to distinguish from surrounding normal tissue[33]. The desired molecular signals can be recorded at high spatial and temporal resolution only if targeted contrast agents provide biomolecular specificity and strong image contrast per molecule.

Molecular imaging has been a clinical reality for some time using targeted radionuclides, with early work in the field leveraging decades of developments in positron emission tomography (PET). While PET has shown that imaging systems can track specific

NIH-PA Author Manuscript

NIH-PA Author Manuscript

NIH-PA Author Manuscript

molecules, its prohibitive cost and limited space-time resolution make it difficult to co-register with anatomical features. Furthermore, the presence of a radioactive agent in the body limits its usage for many applications. The role for PET, MR and optical methods in molecular imaging is being pursued by a number of leading organizations; most molecular imaging research funding is going to these modalities. Several groups have developed targeted paramagnetic nanoparticles with reasonable MRI contrast per molecule and high biologic specificity. For example, a targeted paramagnetic nanoparticle has been used to image tumor neovasculature and angiogenesis associated with atherosclerotic plaque development[34]. Additionally, imaging angiogenesis can help monitor the therapeutic response of anti-angiogenic agents. Optical molecular imaging has been used extensively in mouse models, especially in the area of drug development[24]. However, optical methods suffer from strong light scattering *in vivo*, resulting in poor image depth and limiting use to superficial regions. Translating optical techniques into robust clinical tools may be difficult given these limitations.

Ultrasound Molecular Imaging

While results with other modalities are very promising and will likely offer many health benefits, all modalities will have limits for personalized medicine due to cost, portability, resolution, and depth of penetration. We believe that ultrasound will be one of the major drivers of personalized medicine. Just as in conventional imaging where more ultrasound procedures are performed than any other modality[31], ultrasound must become a primary delivery mechanism for molecular diagnostics, translating the potential of molecular methods into routine clinical procedures.

Not only does ultrasound bring unique strengths that can supplement existing molecular imaging modalities, its wide availability, low operating and capital costs, and real-time operation will be essential to enable molecular diagnosis to transform the way medicine is conducted in this country. Ultrasound enables real-time imaging, and can attain spatial resolution approaching 50 um for many applications, superior to MRI and PET. Due to its high portability and low cost, ultrasound is now one of the leading medical diagnostic tools in the world.

Molecular imaging studies to date with ultrasound have primarily used microbubbles. These bubbles can be coated with polymers or proteins and targeted like other molecular imaging agents[4]. Although initially gas filled, they can also be filled with pharmaceuticals such as chemotherapeutics. In addition to microbubbles, perflourocarbon-based nanoparticles targeted to cell-bound proteins become highly reflective and are detectable by ultrasound[35]. Clinical applications are numerous. For example, angiogenesis is a key biologic step required for tumor invasiveness. Lindner's group reported using ultrasound microbubbles targeted to $\alpha_v\beta_3$ integrin expressed in the endothelium of glioma animal models[4]. Notably, this area of angiogenesis was demonstrated beyond the tumor margins delineated by conventional imaging. A number of therapeutic interventions are targeted at blocking tumor-induced angiogenesis. This technique not only can help evaluate the effectiveness for an individual patient, but it also can be used to assess effectiveness in developing new angiogenesis inhibitors. Quantitating angiogenesis can also help evaluate revascularization procedures, reconstructive surgery, and stem cell therapy. A particular strength of ultrasound is that it does not introduce damaging radiation that might perturb the biologic system being assessed.

Photoacoustic Molecular Imaging

Due to their relatively large size (approximately 1 μm), microbubbles are primarily limited to the vasculature. A complementary molecular imaging approach uses a class of

NIH-PA Author Manuscript

NIH-PA Author Manuscript

NIH-PA Author Manuscript

biologically targeted agents with significant **optical absorption** (i.e., **not** fluorescence) over a limited wavelength range. These agents are similar in size and binding characteristics to natural macromolecules and can provide large contrast per molecule for **photoacoustic** imaging. Photoacoustics combines optical and acoustic methods, where contrast is based on optical absorption and spatial resolution scales with ultrasonic frequency[13, 16]. It is less sensitive to scattering limitations, in contrast to optical imaging, and can provide real-time images at significant image depth with high spatial resolution. The combination of high optical contrast and sub-mm spatial resolution of US detection deep within tissue has made PA imaging a promising tool for molecular imaging[11, 15, 22, 26]. PA imaging has great potential to detect and differentiate specific molecules from other components because it has a unique contrast mechanism, optical absorption, not shared by any other imaging modality. By targeting a designed contrast agent with absorption peak at a specific wavelength to biological objects, such as tumor cells, PA imaging can non-invasively image targeted objects specifically and sensitively, for ultrasound molecular imaging beyond the vascular bed, particularly for early diagnosis of common cancers such as those of the prostate[1, 5, 17, 36].

Integrated Molecular Imaging and Therapy

Molecular imaging and therapy can be integrated, where a biologically targeted agent provides both efficient contrast for molecular imaging and the delivery vehicle for molecular therapeutics. For example, microbubbles can be filled with pharmaceuticals such as chemotherapeutics. High intensity focused ultrasound (HIFU) can then be used to burst targeted microbubbles, releasing the therapeutic agent in a highly controlled way. Similarly, gene therapy can be introduced into a targeted region by incorporating genetic material in microbubbles or nanoparticles. HIFU can generate extreme temperatures in a highly targeted area. Temperature can be used to regulate gene expression, drug transport, and apoptosis. Targeted photoacoustic contrast agents are highly efficient absorbers at a fixed optical wavelength. Consequently, high intensity monochromatic light can initiate highly localized and targeted thermal therapy similar to HIFU[14].

Ultrasound, and the companion modality of photoacoustics, provide cost-effective tools to enable the “virtuous feedback loops” driving the personalized medicine paradigm of Figure 1. We believe that ultrasound can become a primary delivery mechanism for molecular medicine, translating the potential of molecular methods into routine clinical procedures. Below we describe a particular application of molecular imaging with integrated ultrasound/photoacoustic imaging for the detection of rare circulating cells, including circulating tumor cells (CTCs).

Specific Example

Detection and identification of rare cell types circulating in the vasculature is a major challenge for the management of disease using molecular tools. In particular, detection of CTCs represents a significant problem in molecular imaging and, if solved, can significantly impact the management of metastatic disease. Metastasis, where CTCs originating from a primary tumor spread to other organs through blood or lymphatic circulation, causes over 90% of cancer deaths[30]. Detecting CTCs helps in early analysis of tumor cell genetic and pathologic characteristics, and in effective early stage treatment[6]. However, identifying CTCs remains a big challenge due to their rarity in blood. Compared to billions of red blood cells and millions of white blood cells in one ml of blood, there are only 1-10 CTCs on average for an active tumor[20].

Many techniques have been proposed to separate and identify CTCs. Immunomagnetic enrichment with polymer or ferromagnetic beads coated with antibodies bound with cell

NIH-PA Author Manuscript

NIH-PA Author Manuscript

NIH-PA Author Manuscript

surface antigens captures CTCs from blood samples[20]. Microchips and microfluidic devices can help capture, count, and analyze CTCs in blood samples[21]. Filters with precise pore size allow blood cells to pass but retain CTCs[37]. Some procedures also use flow cytometry to sort CTCs by centrifugation and staining identification[25]. Unfortunately, in all these *in vitro* approaches, samples are taken repeatedly by invasive biopsies and bone marrow aspirations. In particular, a limited sample volume (typically 5-10 ml) significantly decreases diagnostic confidence. Furthermore, real-time readout is not possible in such procedures[6].

Non-invasive CTC detection in a small animal model with multiphoton fluorescence imaging has been proposed[7]. However, the shallow penetration depth of this optical method makes it only work on superficial blood vessels, limiting the volume of blood being interrogated in a reasonable procedure time and thus decreasing detection sensitivity. PA imaging, in contrast, has centimeter-scale penetration depth to image peripheral vessels and provides high detection sensitivity by examining relatively large blood volumes over the same time. For example, if the radial or brachial artery can be used, over 100 ml of blood can be analyzed in a 10 minute exam. This means even a crude PA system with a sensitivity of 10 cells yields a procedure sensitivity of 0.1 CTCs/ml! This advantage makes PA imaging an excellent candidate to sensitively detect CTCs of concentration within the typical range (i.e., 1-10 cells/ml) using functionalized contrast agents targeted to a specific CTC.

Unfortunately, intrinsic absorbers, such as tissues and blood, are efficient sources of strong background PA signals, which seriously degrade the sensitivity of detecting targeted molecules or cells. Figure 2 presents an example of PA molecular imaging of a tumor in a living mouse[36]. After intravenous injection of a targeted contrast agent (Figure 2b), cyclic Arg-Gly-Asp (RGD) peptide-coupled carbon nanotubes, the PA signal in the tumor region (the skin and tumor boundaries shown in the ultrasound image, and the active tumor site is noted in the PA images) significantly increases compared to the pre-injection image (Figure 2a), indicating the efficacy of targeted contrast agent recognition of the tumor region. However, non-negligible PA signals generated from the intrinsic absorption of tissue or blood are seen in the pre-injection image. This nonspecific signal decreases detection sensitivity and specificity and makes quantitative measurement almost impossible, especially when diseased tissue approaches the resolution limit of the imaging system, as in a very early stage tumor where the number of cancer cells is small, or for rare CTCs in the vasculature.

Magnetomotive photoacoustic imaging

A new method has been developed recently to increase specific contrast in PA molecular imaging by suppressing background signals from intrinsic absorbers[9, 10, 12, 18, 19, 23, 28]. This technique, called magnetomotive photoacoustic (mmPA) imaging, senses objects labeled with a composite particle combining paramagnetic nanoparticles and an optically absorptive component (e.g., gold nanorods), enabling magnetic manipulation with simultaneous PA detection of the targeted objects. Figure 3 illustrates the mechanism of background suppression in mmPA imaging and its contrast enhancement compared to traditional PA imaging. By biologically coupling the contrast agent to targeted tissues or cells and magnetically manipulating them with an external magnetic field, the targeted region moves coherently with the magnetic field. This movement modulates PA signals either spatially or temporally, enabling subsequent motion filtering on a series of the recorded PA signals to suppress magnetically-insensitive background signals[10, 12, 28]. In the case of detecting CTCs, targeted cells can be magnetically enriched, and differentiated from the blood with the mmPA technique, which is nearly impossible with traditional PA imaging due to the rarity of CTCs in a heterogeneous background with strong scattering and absorption (i.e., blood pool).

NIH-PA Author Manuscript

NIH-PA Author Manuscript

NIH-PA Author Manuscript

Composite contrast agent

An example of a composite mmPA contrast agent consisting of a magnetic nanoparticle (MNP) of 25 nm diameter coated with a gold shell (MNP-gold core-shell)[12] is shown in Figure 4. The gap between the MNP core and gold shell is about 3 nm and the shell thickness varies from 1 nm to 5 nm, resulting in a blue shift of the surface plasmon resonance (SPR) extinction peak from 900 nm to 660 nm[12]. The peak is quite broadband and covers the optical window in biological tissue (800- 1000 nm) and enables maximal light penetration into tissue for PA imaging.

Figure 5a and 5b illustrate a schematic and a transmission electron microscope (TEM) image of an alternative design of a composite contrast agent for mmPA imaging. It combines a gold nanorod (GNR) core with a silica coating layer, which provides a structural scaffold for MNP attachment and increases the photo-thermal stability of the GNR core[3]. The absorption spectra of silica-MNP particles with a diameter equal to the long axis of a GNR (60 nm), silica-encapsulated GNR, and GNR-silica-MNP are compared in Figure 5c. The silica-MNP particles exhibit a relatively lower and decaying absorption profile from 400-1000 nm (purple). The characteristic longitudinal surface plasmon resonance (SPR) peak of GNR-silica before MNP conjugation is at 812 nm (green) and slightly red-shifts to 827 nm after conjugation due to contributions from the MNPs (red), indicating the absorptive characteristic of a GNR-silica-MNP particle is almost unchanged compared to a GNR-silica one. A similar design of hybrid nanostructure combining GNRs and superparamagnetic iron oxide nanoparticles for biomedical imaging and therapy has also been proposed[27].

Results

Proof of principle with phantom experiment

To demonstrate the principle of background suppression in mmPA imaging, a polyvinyl alcohol (PVA) phantom containing three inclusions, 3 nM MNPs, 3 nM MNP-gold core-shell, and GNRs with the same absorption as 3 nM hybrid particles, was imaged with a PA imaging setup and an electromagnet[12]. The magnetic field was toggled during the recording by turning on/off the electromagnet placed under the phantom. The recorded image using traditional PA imaging is shown in figure 6a, in which the regions of GNR (left, representing intrinsic background) and composite particles (center, representing targeted cells) exhibit comparable signal amplitude (displayed on a logarithmic scale over a 40 dB dynamic range). By toggling the electromagnet on/off, MNPs and composite particles move down/up due to gaining/losing the attractive force of the magnetic field. According to the displacement (Figure 6b) obtained based on a pixel-by-pixel motion tracking algorithm using a series of PA images at different magnet phases, a weighting map identifying regions that move coherently with the magnet field can be created (Figure 6c). By multiplying the weighting map with the original PA imaging, the region without magnetic particles is suppressed by more than 40 dB, while the regions with MNPs and composite particles remain unchanged (Figure 6d).

In vitro studies with HeLa cells mimicking CTCs

The potential of detecting CTCs in the vasculature with mmPA imaging was demonstrated with *in vitro* experiments using a human cervical cancer cell line, HeLa, which overexpresses the folate receptor (FR). Cells were targeted with GNR-silica-MNP nanoparticles using folic acid (FA) as a model binding ligand linked to the particles through PEG. As shown in Figure 7, numerous multifunctional composite nanoparticles bind to a CTC, enabling magnetic enrichment of the cell in blood flow with sensitive and specific PA detection[9].

NIH-PA Author Manuscript

NIH-PA Author Manuscript

NIH-PA Author Manuscript

A dual-magnet system built of permanent magnets was designed and fabricated to trap cells flowing in a 1.6 mm tube phantom mimicking a human radial artery. The magnet system consists of two face-to-face flat magnets on opposite sides of the tube providing a homogeneous field to polarize the MNPs, and a cone magnet array producing a sharp gradient field with strong trapping force on the polarized MNPs. The dual-magnet approach provides a potential path to design a practical system which can accumulate CTCs at a flow rate comparable to that in a human radial artery and detect trapped cells with real-time mmPA imaging.

To evaluate targeting specificity and selectivity, cells incubated with four different particles were imaged[9] at a laser fluence of 5.5 mJ/cm^2, as shown in Figure 8. The cell concentration is 5000 cells/ml solution. US pulse-echo signals of the tube walls are displayed in gray scale, and PA signals in hot pseudo color. No PA signals appears in the top two images (Figure 8a and 8b) of cell samples incubated with GNR-silica-FA and silica-MNP-FA, respectively. As illustrated in panels a, although cells can be molecularly targeted with GNR-silica-FA including the FA ligand, they cannot accumulate in the trapping region (above the magnet tip shown as the trapezoid). It functions like a traditional PA imaging system that cannot detect separate cells flowing in the tube because all signals are below the detection limit. For cells reacted with silica-MNP-FA, targeted cells can be trapped. However, the PA signals are still below the detection limit because MNPs have relatively lower optical absorption and thus weaker PA signals. Figure 8c and 8d show cells reacted with composite contrast agents, GNR-silica-MNP, except no FA ligand for the former. The small signal observed in Figure 8c indicates non-specific binding of the composite to cells. With active targeting using the FA ligand, PA signals increase by more than 10 times, showing specific detection of targeted cells with mmPA imaging (Figure 8d). Figure 8e shows the results of testing free (i.e., not bound to cells) contrast agents, GNR-silica-MNP-FA, under the same condition. No free contrast agent was trapped in the magnetic region due to a much weaker magnetic trapping force on a free single agent compared to that on a cell with a large collection of targeted agents, and thus no false-positive signal was produced.

The trapping experiment was repeated with a cell concentration of 1 cell/ml to evaluate the trapping efficiency and detection sensitivity of the current mmPA imaging system[9]. Figure 9 depicts fusion (US+PA) images at different time points during an 80-minute trapping procedure at a 6 ml/min flow rate. During the first 32 minutes, no PA signals can be observed because the signal amplitude from a few trapped cells is still below the detection limit. After 34 minutes, the PA signals increase and several clusters appear, indicating that more and more cells accumulate due to the strong magnet force, which traps the cells and keeps them in the trapping region against the flow drag force. Note that each cell only passes from right to left through the trapping region once, mimicking *in vivo* conditions with a long circulation path and full cell clearance during every blood circle. The trapping efficiency estimated from the ratio of the number of trapped cells over that of total cells (i.e., 1 cell/ml × 6 ml/min × 80 minutes = 480 cells) is about 67%, and the estimated minimum detectable cell number is 136 at 34 minutes, assuming constant trapping efficiency[9].

Figure 10 depicts an example of contrast enhancement through background suppression by repeating the trapping experiment in ink solution with highly absorptive background[29]. Even with a high concentration of 500 cells/ml, the signals from the trapped cells are still masked by the strong background signals from ink, shown in Figure 10a and 10b with the magnet at different positions. Nevertheless, applying a simple form of motion filtering, subtraction between the two images, extracts the components that move with the magnet (i.e., trapped cells) but eliminates static background signals and moving objects insensitive to the magnet field. By comparing the contrast between ink signals along the top wall and trapped cells signals before (Fig. 10a and b) and after (Fig. 10(c)) image subtraction, the detection

NIH-PA Author Manuscript

NIH-PA Author Manuscript

NIH-PA Author Manuscript

contrast increases by more than 16 dB, demonstrating the advantage of mmPA imaging over traditional PA imaging for ultrasensitive probing at the cellular (e.g., CTCs) and molecular level in a heterogeneous environment with a strong interfering background.

The next step in these studies will focus on detecting CTCs *in vivo* using mmPA imaging of a well-developed metastasis model in small animals. A more robust magnet trapping design integrated with a more sensitive real-time US/PA imaging system is the near-term goal before translating the current technology toward clinical applications.

Conclusions

Molecular imaging has the potential to shape the emerging field of personalized medicine, probing molecular abnormalities that drive disease processes rather than the consequences of these molecular alterations. Highly sensitive and specific localization of molecular probes will be very important in both diagnostic molecular imaging and image-guided molecular therapies. In this review, we have presented a particular example of molecular imaging that could significantly affect the management of metastatic disease.

A new modality, magnetomotive photoacoustic imaging, provides the molecular sensitivity of optical contrast agents combined with the deep penetration and high *in vivo* spatial resolution of ultrasound to produce images of molecularly targeted CTCs even in the presence of significant background signals from efficient optical absorbers such as blood. Results obtained *in vitro* demonstrated that this technology is capable of detecting CTCs at a concentration as low as one cell per ml of blood. Future studies will be directed at translating mmPA into a robust clinical tool applicable to a wide range of applications in molecular diagnostics.

Acknowledgments

This work was supported in part by NIH RO1EB016034, RO1CA170734, RO1CA131797, R01CA140295, T32CA138312, NSF 0645080, the Life Sciences Discovery Fund 3292512, and the Department of Bioengineering at the University of Washington.

References

1. Agarwal A, Huang SW, O'Donnell M, Day KC, Day M, Kotov N, Ashkenazi S. Targeted gold nanorod contrast agent for prostate cancer detection by photoacoustic imaging. J. Appl. Phys. 2007; 102:064701.
2. Centers for Medicare & Medicaid Services, Office of the Actuary. National Health Expenditure Projections. 2012. 2011-2021:http://www.cms.gov/Research-Statistics-Data-and-Systems/Statistics-Trends-and-Reports/NationalHealthExpendData/Downloads/Proj2011PDF.pdf
3. Chen L-C, Wei CW, Souris JS, Cheng SH, Chen CT, Yang CS, Li PC, Lo LW. Enhanced photoacoustic stability of gold nanorods by silica matrix confinement. J. Biomed. Opt. 2010; 15:016010. [PubMed: 20210456]
4. Ellegala DB, Leong-Poi H, Carpenter JE, Klibanov AL, Kaul S, Shaffrey ME, Sklenar J, Lindner JR. Imaging tumor angiogenesis with contrast ultrasound and microbubbles targeted to $\alpha_v\beta_3$. Circulation. 2003; 108:336–341. [PubMed: 12835208]
5. Emelianov SY, Li PC, O'Donnell M. Photoacoustics for molecular imaging and therapy. Phys. Today. 2009; 62(5):34–39. [PubMed: 20523758]
6. Fleisher M. A new opportunity for therapeutic management of cancer patients. Clin. Lab. News. 34(11):2008.
7. He W, Wang H, Hartmann LC, Cheng JX, Low PS. In vivo quantitation of rare circulating tumor cells by multiphoton intravital flow cytometry. Proc. Natl. Acad. Sci. USA. 2007; 104:11760–11765. [PubMed: 17601776]

NIH-PA Author Manuscript

NIH-PA Author Manuscript

NIH-PA Author Manuscript

8. Hood L, Heath JR, Phelps ME, Lin B. Systems biology and new technologies enable predictive and preventative medicine. Science. 2004; 306:640–643. [PubMed: 15499008]
9. Hu X, Wei CW, Xia J, Pelivanov I, O'Donnell M, Gao X. Trapping and photoacoustic detection of CTCs at the single cell per milliliter level with magneto-optical coupled nanoparticles. Small. 2012 DOI: 10.1002/smll.201202085.
10. Jia C, Huang SW, Jin Y, Seo CH, Huang L, Eary JF, Gao X, O'Donnell M. Integration of photoacoustic, ultrasound, and magnetomotive system. Proc. SPIE 7564, Photons Plus Ultrasound: Imaging and Sensing. 2010:756416. doi:10.1117/12.842485.
11. Jin X, Li CH, Wang LV. Effects of acoustic heterogeneities on transcranial brain imaging with microwave-induced thermoacoustic tomography. Med. Phys. 2008; 35(7):3205–3214. [PubMed: 18697545]
12. Jin Y, Jia C, Huang SW, O'Donnell M, Gao X. Multifunctional nanoparticles as coupled contrast agents. Nat. Commun. 2010; 1:41. [PubMed: 20975706]
13. Karabutov AA, Podymova NB, Letokhov VS. Time-resolved laser optoacoustic tomography of inhomogeneous media. Appl. Phys. B-lasers O. 1996; 63(6):545–563.
14. Lapotko D, Lukianova-Hleb E, Zhdanok S, Rostro B, Simonette R, Hafner J, Konopleva M, Andreeff M, Conjusteau A, Oraevsky A. Photothermolysis by laser-induced microbubbles generated around gold nanorod clusters selectively formed in leukemia cells. Proc. SPIE 6856, Photons Plus Ultrasound: Imaging and Sensing. 2008:68560K. doi: 10.1117/12.771660.
15. Larina IV, Larin KV, Esenaliev RO. Real-time optoacoustic monitoring of temperature in tissues. J. Phys. D: Appl. Phys. 2005; 38(15):2633–2639.
16. Li C, Wang LV. Photoacoustic tomography and sensing in biomedicine. Phys. Med. Biol. 2009; 54(19):R59–R97. [PubMed: 19724102]
17. Li PC, Wang CRC, Shieh DB, Wei CW, Liao CK, Poe C, Jhan S, Ding AA, Wu YN. In vivo photoacoustic molecular imaging with simultaneous multiple selective targeting using antibody-conjugated gold nanorods. Opt. Express. 2008; 16(23):18605–18615. [PubMed: 19581946]
18. Mehrmohammadi M, Yoon KY, Qu M, Johnston KP, Emelianov SY. Enhanced pulsed magneto-motive ultrasound imaging using superparamagnetic nanoclusters. Nanotechnol. 2011; 22:045502.
19. Mehrmohammadi M, Oh J, Mallidi S, Emelianov SY. Pulsed magneto-motive ultrasound imaging using ultrasmall magnetic nanoprobes. Mol. Imaging. 2011; 10(2):102–110. [PubMed: 21439255]
20. Miller C, Doyle GV, Terstappen LWMM. Significance of circulating tumor cells detected by the cell search system in patients with metastatic breast colorectal and prostate cancer. J. Oncol. 2010 2010: doi:10.1155/2010/617421.
21. Nagrath S, Sequist LV, Maheswaran S, Bell D, Irimia D, Ulkus L, Smith MR, Kwak EL, Digumarthy S, Muzikansky A, Ryan P, Balis UJ, Tompkins RG, Ha AD. Isolation of rare circulating tumour cells in cancer patients by microchip technology. Nat. 2007; 450:1235–1239.
22. Pramanik M, Ku G, Li CH, Wang LV. Design and evaluation of a novel breast cancer detection system combining both thermoacoustic (TA) and photoacoustic (PA) tomography. Med. Phy. 2008; 35(6):2218–2223.
23. Qu M, Mallidi S, Mehrmohammadi M, Truby R, Homan K, Joshi P, Chen Y-S, Sokolov K, Emelianov SY. Magneto-photo-acoustic imaging. Biomed. Opt. Express. 2011; 2(2):385–395. [PubMed: 21339883]
24. Rudin M, Weissleder R. Molecular imaging in drug discovery and development. Nature Reviews Drug Discovery. 2003; 2:123–131.
25. Shaffer R, Leversha MA, Danila DC, Lin O, Gonzalez-Espinoza R, Gu B, Anand A, Smith K, Maslak P, Doyle GV, Terstappen LW, Lilja H, Heller G, Fleisher M, Scher HI. Circulating tumor cell analysis in patients with progressive castration-resistant prostate cancer. Clin. Cancer Res. 2007; 13:2023–2029. [PubMed: 17404082]
26. Talbert RJ, Holan SH, Viator JA. Photoacoustic discrimination of viable and thermally coagulated blood using a two-wavelength method for burn injury monitoring. Phys. Med. Biol. 2007; 52(7): 1815–1829. [PubMed: 17374913]
27. Truby RL, Emelianov SY, Homan KA. Ligand-mediated self-assembly of hybrid plasmonic and superparamagnetic nanostructures. Langmuir. 2013; 29:2465–70. [PubMed: 23362922]

NIH-PA Author Manuscript

NIH-PA Author Manuscript

NIH-PA Author Manuscript

28. Wei C-W, Xia J, Pelivanov I, Hu X, Gao X, O'Donnell M. Trapping and dynamic manipulation of polystyrene beads mimicking circulating tumor cells using targeted magnetic/photoacoustic contrast agents. J. Biomed. Opt. 2012; 17(10):101517. [PubMed: 23223993]
29. Wei CW, Xia J, Pelivanov I, Hu X, Gao X, O'Donnell M. Magnetic trapping with simultaneous photoacoustic detection of molecularly targeted rare circulating tumor cells. Proc. SPIE 8581, Photons Plus Ultrasound: Imaging and Sensing. 2013:85814W. doi:10.1117/12.2008969.
30. Weigelt B, Peterse JL, van 't Veer LJ. Breast cancer metastasis: markers and models. Nat. Rev. Cancer. 2005; 5:591–602. [PubMed: 16056258]
31. Wells PNT. Physics and engineering: milestones in medicine. Med. Eng. Phys. 2001; 23:147–153. [PubMed: 11410379]
32. Weston AD, Hood L. Systems biology, proteomics, and the future of health care: toward predictive, preventative, and personalized medicine. J. Proteome Res. 2004; 3(2):179–96. [PubMed: 15113093]
33. Wickline SA, Lanza GM. Nanotechnology for Molecular Imaging and Targeted Therapy. Circulation. 2003; 107:1092–1095. [PubMed: 12615782]
34. Wickline SA, Neubauer A,M, Winter PM, Caruthers SD, Lanza GM. Molecular imaging and therapy of atherosclerosis with targeted nanoparticles. J Magn. Reson. Imaging. 2007; 25:667–680. [PubMed: 17347992]
35. Winter PM, Cai K, Caruthers SD, Wickline SA, Lanza GM. Emerging nanomedicine opportunities with perflourocarbon nanoparticles. Expert Rev. Med. Devices. 2007; 4:137–145. [PubMed: 17359221]
36. Zerda A, Liu Z, Bodapati S, Teed R, Vaithilingam S, Khuri-Yakub BT, Chen X, Dai H, Gambhir SS. Ultrahigh sensitivity carbon nanotube agents for photoacoustic molecular imaging in living mice. Nano Lett. 2010; 10:2168–2172. [PubMed: 20499887]
37. Zhenga S, Linb H, Liua JQ, Balicb M, Datarb R, Coteb RJ, Tai YC. Membrane microfilter device for selective capture, electrolysis and genomic analysis of human circulating tumor cells. J. Chromatogr. A. 2007; 1162(2):154–161. [PubMed: 17561026]

NIH-PA Author Manuscript

NIH-PA Author Manuscript

NIH-PA Author Manuscript

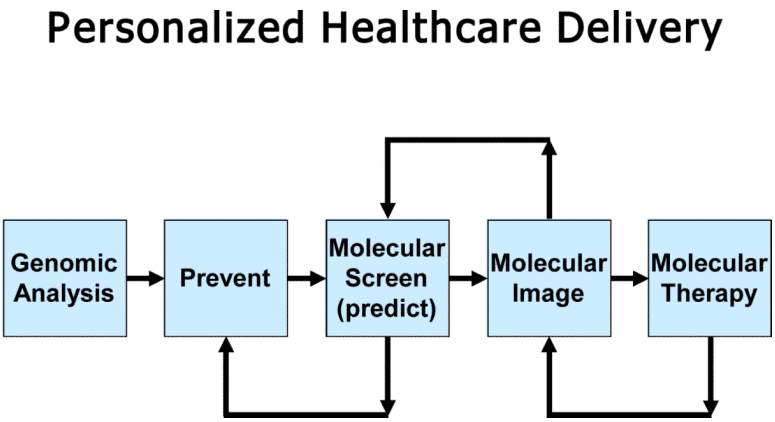

Figure 1.
Block diagram of personalized healthcare delivery.

NIH-PA Author Manuscript

NIH-PA Author Manuscript

NIH-PA Author Manuscript

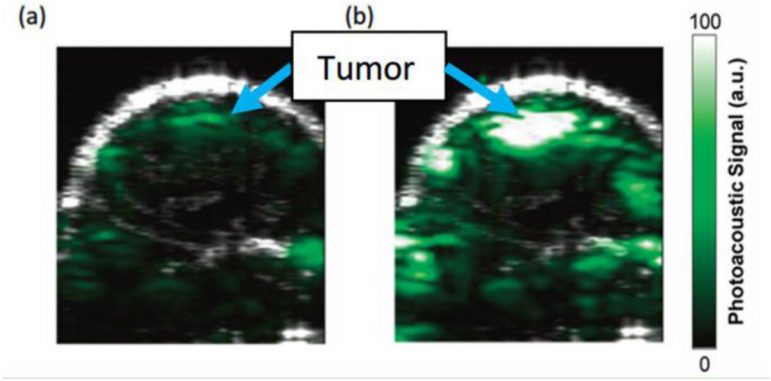

Figure 2.

Images of a tumor in a living mouse showing ultrasound signal (gray) and photoacoustic signal (green)[36]. The ultrasound images show the skin and the tumor boundaries. Arrows show where the tumor is highlighted in the photoacoustic images. (a) Image before injection, and (b) image at 2 hours after injection with contrast agents targeted to tumor vasculature. Reprinted with permission from (Zerda, A., Z. Liu, S. Bodapati, R. Teed, S. Vaithilingam, B. T. Khuri-Yakub, X. Chen, H. Dai, and S. S. Gambhir. Ultrahigh sensitivity carbon nanotube agents for photoacoustic molecular imaging in living mice. *Nano Lett.* 10:2168-2172, 2010). Copyright (2010) American Chemical Society.

NIH-PA Author Manuscript

NIH-PA Author Manuscript

NIH-PA Author Manuscript

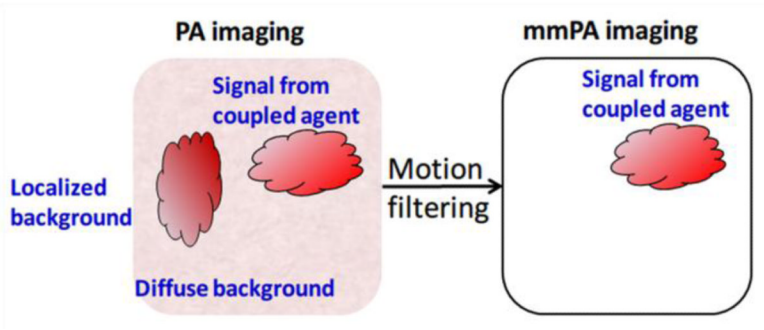

Figure 3.
Mechanism of background suppression using mmPA technique[12]. Background regions without magnetic contrast agents are suppressed due to their non-susceptibility to a controlled magnetic field, while regions with coupled agents responsive to a magnetic field are preserved. Reprinted by permission from Macmillan Publishers Ltd: [Nature Communications] (Jin, Y., C. Jia, S. W. Huang, M. O'Donnell, and X. Gao. Multifunctional nanoparticles as coupled contrast agents. *Nat. Commun*. 1:41, 2010), copyright (2010).

NIH-PA Author Manuscript

NIH-PA Author Manuscript

NIH-PA Author Manuscript

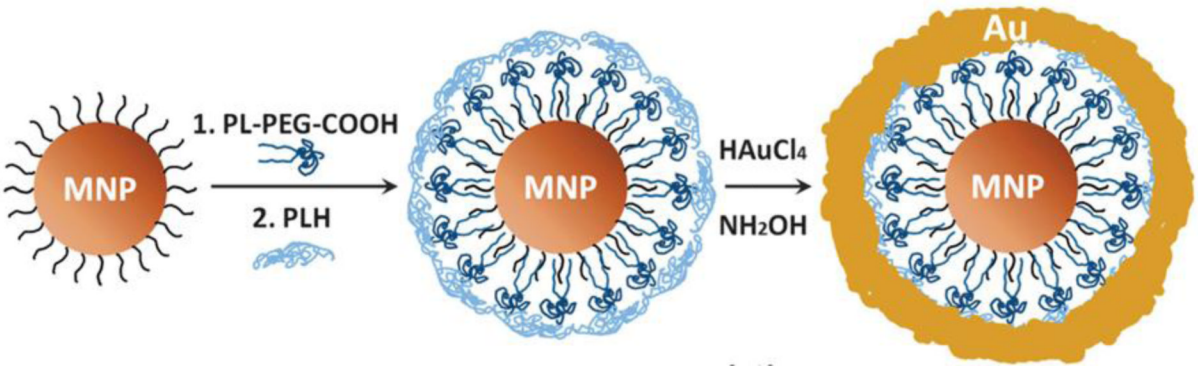

Figure 4.

Schematic of synthesis approach for MNP-gold core-shell NPs[12]. Reprinted by permission from Macmillan Publishers Ltd: [Nature Communications] (Jin, Y., C. Jia, S. W. Huang, M. O'Donnell, and X. Gao. Multifunctional nanoparticles as coupled contrast agents. Nat. Commun. 1:41, 2010), copyright (2010).

NIH-PA Author Manuscript

NIH-PA Author Manuscript

NIH-PA Author Manuscript

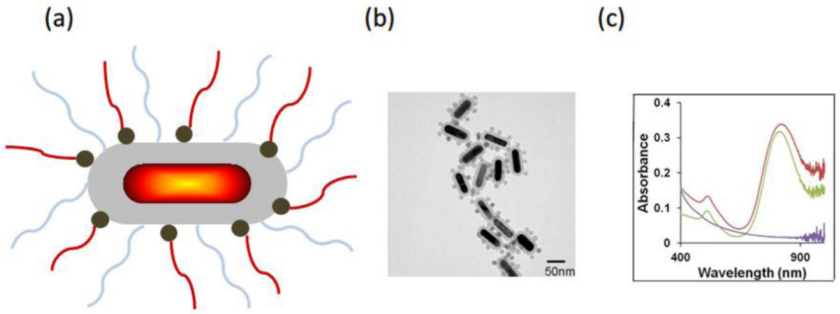

Figure 5.

Composite contrast agent combining a GNR core with silica coating and MNPs[9]. (a) Schematic illustration and (b) TEM images of GNR-silica-MNP particles. (c) Ultraviolet-visible spectra of GNR-silica-MNP particles (red), silica-encapsulated GNR (green), and silica-MNP particles with 60 nm diameter (purple). Reprinted with permission from (Hu X., C. W. Wei, J. Xia, I. Pelivanov, M. O'Donnell, and X. Gao. Trapping and photoacoustic detection of CTCs at the single cell per milliliter level with magneto-optical coupled nanoparticles. *Small*. DOI: 10.1002/smll.201202085, 2012). Copyright (2012) John Wiley and Sons.

NIH-PA Author Manuscript

NIH-PA Author Manuscript

NIH-PA Author Manuscript

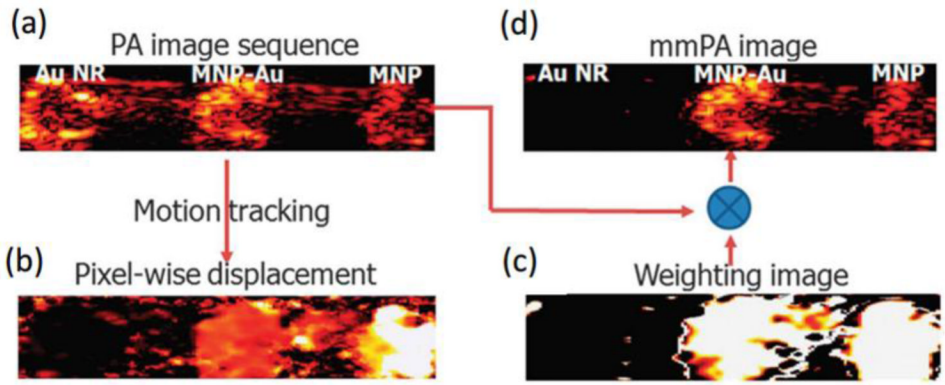

Figure 6.

Data processing in mmPA imaging of a PVA phantom with inclusions of GNRs (left), MNP-gold core-shell (center), and MNPs (right)[12]. (a) Traditional PA image. (b) Maximum displacement corresponding to the magnetic field action. (c) Weighting image based on the displacement. (d) mmPA image produced by multiplying (a) and (c). Reprinted by permission from Macmillan Publishers Ltd: [Nature Communications] (Jin, Y., C. Jia, S. W. Huang, M. O'Donnell, and X. Gao. Multifunctional nanoparticles as coupled contrast agents. *Nat. Commun*. 1:41, 2010), copyright (2010).

NIH-PA Author Manuscript
NIH-PA Author Manuscript
NIH-PA Author Manuscript

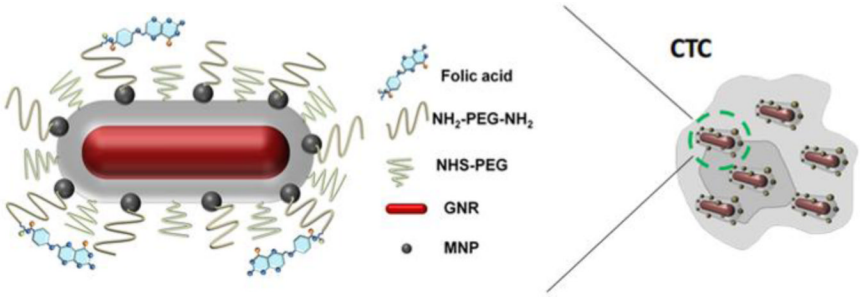

Figure 7.

Composite GNR-silica-MNP contrast agent molecularly targeted to a CTC[9]. Reprinted with permission from (Hu X., C. W. Wei, J. Xia, I. Pelivanov, M. O'Donnell, and X. Gao. Trapping and photoacoustic detection of CTCs at the single cell per milliliter level with magneto-optical coupled nanoparticles. *Small*. DOI: 10.1002/smll.201202085, 2012). Copyright (2012) John Wiley and Sons.

NIH-PA Author Manuscript
NIH-PA Author Manuscript
NIH-PA Author Manuscript

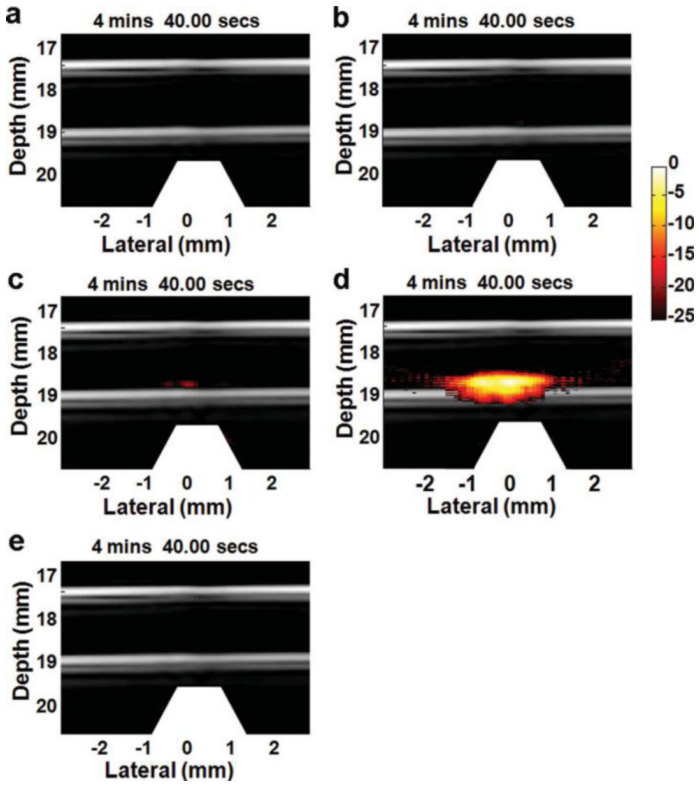

Figure 8.

Fusion images (US and PA – 25 dB log scale) of captured HeLa cells showing targeting specificity and selectivity[9]. The cells are labeled with (a) GNR-silica-FA, (b) silica-MNP-FA, (c) GNR-silica-MNP, and (d) GNR-silica-MNP-FA. (e) Free GNR-silica-MNP-FA probes are not trapped in the magnetic zone. Reprinted with permission from (Hu X., C. W. Wei, J. Xia, I. Pelivanov, M. O'Donnell, and X. Gao. Trapping and photoacoustic detection of CTCs at the single cell per milliliter level with magneto-optical coupled nanoparticles. *Small*. DOI: 10.1002/smll.201202085, 2012). Copyright (2012) John Wiley and Sons.

NIH-PA Author Manuscript

NIH-PA Author Manuscript

NIH-PA Author Manuscript

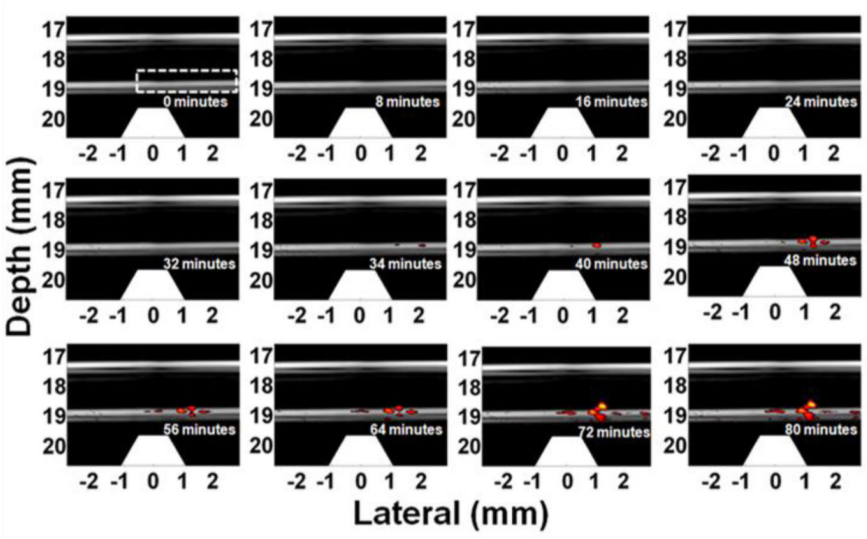

Figure 9.

US/PA images (20 dB log scale) showing accumulation of HeLa cells targeted with GNR-silica-MNPs at 1 cell/ml concentration[9]. Trapezoids below the tube indicate the magnets. Reprinted with permission from (Hu X., C. W. Wei, J. Xia, I. Pelivanov, M. O'Donnell, and X. Gao. Trapping and photoacoustic detection of CTCs at the single cell per milliliter level with magneto-optical coupled nanoparticles. *Small*. DOI: 10.1002/smll.201202085, 2012). Copyright (2012) John Wiley and Sons.

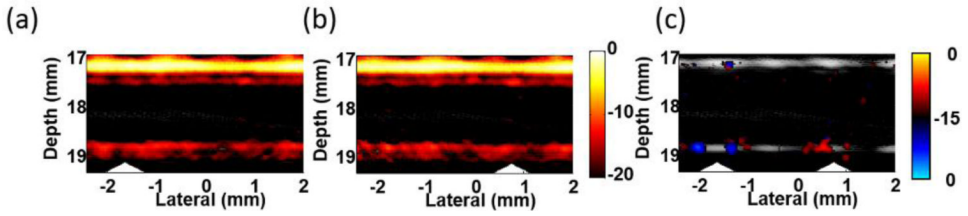

Figure 10.

Images of trapped cells targeted with GNR-silica-MNPS in a highly absorptive solution showing background suppression by changing the location of the trapping magnet[29]. (a) and (b) acquired with the cone magnet array at left and right, respectively. (c) Differential image (bipolar, 15 dB log scale) of (a) and (b). Triangles indicate the magnet positions.

NIH-PA Author Manuscript
NIH-PA Author Manuscript
NIH-PA Author Manuscript